

High-precision real-space simulation of electrostatically-confined few-electron states

Christopher R. Anderson,^{1,2} Mark F. Gyure,^{2,3} Sam Quinn,³ Andrew Pan,³ Richard S. Ross,^{3, a)} and Andrey A. Kiselev³

¹⁾*Department of Mathematics, University of California, Los Angeles, Los Angeles, CA 90095 USA*

²⁾*Center for Quantum Science and Engineering, University of California, Los Angeles, Los Angeles, CA 90095 USA*

³⁾*HRL Laboratories, LLC, 3011 Malibu Canyon Road, Malibu, California 90265, USA*

(Dated: 2 March 2022)

In this paper we present a computational procedure that utilizes real-space grids to obtain high precision approximations of electrostatically confined few-electron states such as those that arise in gated semiconductor quantum dots. We use the Full Configuration Interaction (FCI) method with a continuously adapted orthonormal orbital basis to approximate the ground and excited states of such systems. We also introduce a benchmark problem based on a realistic analytical electrostatic potential for quantum dot devices. We show that our approach leads to highly precise computed energies and energy differences over a wide range of model parameters. The analytic definition of the benchmark allows for a collection of tests that are easily replicated, thus facilitating comparisons with other computational approaches.

Keywords: quantum dot, simulation, full configuration interaction, exchange interaction

1. INTRODUCTION

Semiconductor spin qubits show great promise for quantum information applications.^{1–3} They rely on precise control of the spatial and spin structure of few-electron quantum dot states. The quantum dots are often realized in planar semiconductor heterostructures where the electrons are confined out-of-plane by a quantum well or metal-oxide-semiconductor (MOS) interface, and in-plane by the electrostatic potential due to voltage-biased gate electrodes. In single- or multi-qubit devices, information is contained within quantum dot states whose relevant energy splittings can span a wide range from sub-neV to meV. In particular, a crucial ingredient for many types of spin qubits is the Heisenberg exchange interaction, J , between nearby electrons. Exchange can be used for generating two-qubit gates between individual spins or for controlling a single encoded qubit defined in a multi-spin system. In the absence of an external magnetic field, the exchange energy for two electrons is equal to the energy gap between the ground (singlet) and first excited (triplet) states and can be tuned over many orders of magnitude by changes in the electrostatic potential induced by gate voltage adjustments.⁴

High-precision calculations of the structure of low-energy levels are therefore necessary to simulate the physics and improve understanding and design of spin qubit devices. This requires finding convergent solutions of the N -particle Schrödinger equation, accounting for realistic electrostatic confinement and the electron-electron Coulomb interaction. The full configuration interaction (FCI) method is a powerful approach for solving this problem, capable of providing accurate numerical solutions for the ground and excited states of such systems. First developed in the context of quantum chemistry, it has been increasingly adopted

for analyzing quantum dots,^{5,6} donors,^{7,8} and other artificial few-electron systems,⁹ enabling illuminating studies into their level structure,^{10,11} susceptibility to charge noise^{12,13} and disorder,¹⁴ relaxation rates,¹⁵ and operating regimes for mediated exchange¹⁶ and microwave coupling.¹⁷ The FCI method constructs approximate N -particle solutions from a finite set of orbital basis functions. The number and quality of these orbital basis functions should be chosen well for precise, computationally efficient, and physically representative simulations. Many quantum dot calculations use a set of analytical basis functions and simple confinement models like parabolic or quartic potentials. However, because quantum dot states are strongly dependent on the confining potential, realistic electrostatic potentials, typically obtained as numerical solutions of Poisson's equation, should preferentially be used along with basis functions that reflect the key features of those potentials.

In this work, we present an approach to FCI calculations tailored for simulating realistic quantum dot devices with high precision. In particular, it enables an accurate tracking of the exchange over many orders of magnitude as gate biases are varied — a much more stringent test of simulation capabilities than requiring a high precision value of J for a single bias configuration. We use a real space grid approximation framework to accommodate arbitrary confining potentials. Special consideration is given to the construction of adaptive, orthonormal orbital basis functions and the evaluation of one- and two-particle integrals on those grids.

In order to validate our computational procedure we present results on a benchmark problem that captures the full range of realistic quantum dot operation, ranging from situations of weakly interacting electrons, relatively isolated in individual quantum dots, to cases where they all may be confined in a single quantum dot. This benchmark problem is a good approximation to the potentials associated with the modulation of states in a double quantum dot configuration. A key feature of this benchmark problem is that the potential is a parameterized analytic function, an aspect that greatly facilitates as-

^{a)}Current address: Department of Physics, University of California, Los Angeles, Los Angeles, CA 90095 USA

sessing the accuracy of the FCI simulations over a range of realistic conditions.

In the next section we describe the general FCI procedure for computing solutions to the N -particle Schrödinger equation and present the details of our grid-based implementation of its steps. The benchmark problem is described in the third section, and in the fourth section we present the results obtained using the grid-based computational procedure for this benchmark problem.

2. GRID BASED FULL CONFIGURATION INTERACTION (FCI) PROCEDURE

The computational procedures presented in this paper are described in the context of a completely grid based computational method for determining the eigenfunctions and eigenvalues of a few-electron Hamiltonian associated with the effective mass approximation for electron states within a semiconductor. This problem takes the form $H\Psi = \lambda\Psi$ where the Hamiltonian, H , is the linear operator

$$H = \sum_{i=1}^N \left[\underbrace{-\frac{\hbar^2}{2} \nabla_i \cdot \beta \cdot \nabla_i + U(\mathbf{r}_i)}_{h_i} \right] + \sum_{i=1}^N \sum_{j>i}^N \frac{\alpha}{|\mathbf{r}_i - \mathbf{r}_j|} \quad (1)$$

and $\Psi = \Psi(\tilde{r}_1, \tilde{r}_2, \dots, \tilde{r}_N)$ is the N -particle eigenfunction; $\tilde{r}_i = (\mathbf{r}_i, s_i)$ with $\mathbf{r}_i \in \mathbb{R}^3$ being the spatial coordinate and s_i being the spin coordinate of the i th particle. The external potential U and the reciprocal effective mass tensor β , chosen with $\text{diag} \beta = (m_x^{-1}, m_y^{-1}, m_z^{-1})$, define the single-particle Hamiltonian h (we ignore magnetic fields and spin-orbit effects in this paper, making h and H spin independent). In SI notation, $\alpha = e^2/4\pi\epsilon$ where e is the electron charge and ϵ is the absolute macroscopic static dielectric constant of the semiconductor material. The effective mass model and coordinate-independent values for β and ϵ suffice for describing the main properties of interest in this paper. However, we note that the FCI methodology can be extended beyond the effective mass approximation to use a multi-band model such as $\mathbf{k} \cdot \mathbf{p}$ or tight-binding Hamiltonians, which can be important for simulating valence band holes, valley and spin-orbit physics in silicon devices, or other band structure effects.^{10,18,19} Similarly, coordinate-dependent β and ϵ values, usually present in semiconductor heterostructures, can also be accommodated in our approach with proper attention to underlying subtleties.²⁰

In addition to being an eigenfunction of H , fermionic Ψ must be anti-symmetric with respect to the interchange of any pair of electrons $p, q \in 1 \dots N$:

$$\Psi(\dots, \tilde{r}_p, \dots, \tilde{r}_q, \dots) = -\Psi(\dots, \tilde{r}_q, \dots, \tilde{r}_p, \dots).$$

This brings a non-trivial spin dependence to the multi-electron eigenspectrum even when H is spin independent.

The general methodology that underlies the computational procedure described here is a full configuration interaction (FCI) procedure using orthonormal spatial orbitals.²¹ Assuming a set of M orthonormal functions of \mathbb{R}^3 , “an orbital basis

set”, $\{\phi_j\}_{j=1}^M$, and two orthonormal functions of the spin coordinate, $|\uparrow\rangle$ and $|\downarrow\rangle$, one constructs the $2M$ “spin orbitals”

$$\chi_{2j-1}(\tilde{r}) = \phi_j(\mathbf{r})|\uparrow\rangle, \chi_{2j}(\tilde{r}) = \phi_j(\mathbf{r})|\downarrow\rangle \quad (2)$$

for $j = 1, \dots, M$. One can then construct a N -electron basis function as a Slater determinant

$$v(\tilde{r}_1, \dots, \tilde{r}_N) = \frac{1}{\sqrt{N!}} \det \begin{pmatrix} \chi_1(\tilde{r}_1) & \dots & \chi_1(\tilde{r}_N) \\ \vdots & \ddots & \vdots \\ \chi_N(\tilde{r}_1) & \dots & \chi_N(\tilde{r}_N) \end{pmatrix}$$

where we have selected a distinct subset of $N \leq 2M$ spin orbitals and relabeled the indices of these selected χ 's to run from 1 to N . By construction, each Slater determinant basis function satisfies the requisite anti-symmetry properties of fermions. Also, since the spin orbitals are orthogonal, the resulting full set of $K = \binom{2M}{N}$ distinct Slater determinant basis functions is an orthonormal set.

From a computational perspective, the FCI procedure consists of using a Rayleigh-Ritz method to approximate eigenfunctions and eigenvalues of H given by Eq. (1). One starts with a collection of K orthonormal Slater determinant basis functions $\{v_j\}_{j=1}^K$ and seeks approximate eigenfunctions that are linear combinations of them. The vectors of coefficients $\mathbf{c} = (c_1, \dots, c_K)$ in the expansions of the approximate eigenfunctions are determined by finding the eigenvectors and eigenvalues of the finite dimensional linear system $\tilde{H}\mathbf{c} = \lambda\mathbf{c}$ which is the projection of the operator H onto the subspace formed from the v_j 's, i.e., the (i, j) entry of \tilde{H} , \tilde{H}_{ij} , is given by $\tilde{H}_{ij} = \langle v_i | H | v_j \rangle$. The accuracy of the approximation is improved by expanding the number M of spin orbital basis functions, and, consequently, the number K of Slater determinant basis functions that can be formed from these spin orbitals. Because each Slater determinant is characterized by the projection of total spin S_z , FCI eigenstates of distinct S_z are constructed only using Slater determinants of that projection. This improves the computational efficiency as the subset of Slater determinants for each S_z is reduced.

2.1. Computational Tasks

A principal computational task associated with the FCI procedure, and with wave function based methods in general, is the evaluation of inner products involving Slater determinant basis functions, $\langle v_i | H | v_j \rangle$. These inner products are integrals over the $3N$ spatial coordinates and the N spin coordinates of the N -particle wave function. However, as described in Ref. 21, since Slater determinant basis functions are linear combinations of products of spin orbitals, the task of evaluating these inner products can be reduced to the task of combining the results of the evaluation of integrals over \mathbb{R}^3 and over \mathbb{R}^6 . The integrals over \mathbb{R}^3 are known as “one-electron integrals” and, for real valued orbitals, have the form

$$I_{ij} = \int_{\mathbb{R}^3} \phi_i(\mathbf{r}) h \phi_j(\mathbf{r}) d\mathbf{r} \quad (3)$$

and must be evaluated for all $j \geq i, i = 1, \dots, M$ pairs of spatial orbital basis functions that are used to create the Slater determinant basis functions. Equations simplify further when the eigenfunctions of the single particle Hamiltonian are chosen as the orbitals.

The integrals over \mathbf{R}^6 are known as “two-electron integrals” and have the form

$$I_{ijkl} = \alpha \int_{\mathbf{R}^6} \frac{\phi_i(\mathbf{r}) \phi_j(\mathbf{r}) \phi_k(\mathbf{r}') \phi_l(\mathbf{r}')}{|\mathbf{r} - \mathbf{r}'|} d\mathbf{r} d\mathbf{r}'. \quad (4)$$

These integrals are evaluated for all $j \geq i, i = 1, \dots, M$ pairs and all $l \geq k, k = 1, \dots, M$ pairs of spatial orbitals.

A challenge in the construction of grid based numerical methods is that of efficiently and accurately approximating the values of integrals in Eqs. (3) and (4) when the spatial orbitals ϕ_i are discrete, e.g., they are grid based spatial orbitals.

For computational efficiency we seek approximations that utilize a computational region that is rectangular and a grid that has a uniform mesh in each direction. For optimal accuracy and efficiency, different mesh spacings Δ_γ in each of the coordinate directions $\gamma = x, y, z$ are often used. With this choice of computational domain and grid, one must design accurate approximations to Eqs. (3) and (4). As explained below, the evaluation of the two-electron integrals in Eq. (4) can (and should) avoid the direct evaluation of six dimensional integrals.

We use here the standard multi-dimensional trapezoidal method. We assume that the spatial orbital basis functions vanish outside the computational domain so that the trapezoidal method will be just a simple uniform weight sum of function values over all mesh points, e.g.,

$$\int_{\mathbf{R}^3} f(\mathbf{r}) g(\mathbf{r}) d\mathbf{r} \approx \Delta_x \Delta_y \Delta_z \sum_i \sum_j \sum_k f_{ijk} g_{ijk}. \quad (5)$$

For functions that vanish at the boundaries, the trapezoidal method itself is “infinite order accurate”, i.e., the convergence improves as a product of positive powers of the mesh spacings, with exponents dependent on the smoothness of the integrand.²²

1. One-electron Integrals

In the construction of the approximation of the one-electron integrals Eq. (3) we assume that the spatial orbitals, ϕ_i , are known, are well resolved by the computational grid, and vanish outside the computational domain (the construction of a set of functions with these properties is described below). The first integral in Eq. (3), due to the kinetic term in h , requires the evaluation of $\phi_i(\mathbf{r}) \nabla \cdot \beta \cdot \nabla \phi_j(\mathbf{r})$. The difference operators in this term are approximated with standard high order centered finite differences.²³ The integration of the potential term $\phi_i(\mathbf{r}) U(\mathbf{r}) \phi_j(\mathbf{r})$ in Eq. (3) is straightforward using a trapezoidal method. If the orbital basis functions are smooth functions and vanish outside of the domain, and if the external potential is also smooth, then both kinetic and potential terms in Eq. (3) can be approximated with high accuracy.

2. Two-electron Integrals

The method for computing two-electron integrals is based on the observation that the evaluation of the six dimensional integral I_{ijkl} in Eq. (4) only requires the evaluation of three dimensional operators. As a result, the computational procedure consists of a double loop in which the inner loop evaluates integrals of the form

$$\Phi_{ij}(\mathbf{r}') = \alpha \int_{\mathbf{R}^3} \frac{\phi_i(\mathbf{r}) \phi_j(\mathbf{r})}{|\mathbf{r} - \mathbf{r}'|} d\mathbf{r} \quad (6)$$

at the nodes of the computational grid, and an outer loop where the complete integral is evaluated by forming a trapezoidal approximation to the integral

$$I_{ijkl} = \int_{\mathbf{R}^3} \Phi_{ij}(\mathbf{r}') \phi_k(\mathbf{r}') \phi_l(\mathbf{r}') d\mathbf{r}'. \quad (7)$$

The primary computational difficulty in the evaluation of the two-electron integrals is thus in evaluating Eq. (6). Since these integrals must be evaluated at each grid point of the computational domain, this task is equivalent to determining at all those points the solution to the Poisson equation

$$\Delta \Phi_{ij} = -4\pi\alpha \phi_i \phi_j \quad (8)$$

with “infinite” boundary conditions.

This is a fundamental problem of computational physics and there are many highly efficient algorithms that may be employed. The method one chooses depends upon several factors: the properties of the source functions, available computational hardware, accuracy requirements, etc. For the particular problem presented in this paper the orbital basis functions are not in general strongly localized, and most importantly, the orbital basis functions are not known analytically. The method used here combines two parts: a high order accurate solution of Poisson’s equation obtained using discrete sine transforms, and a high order accurate finite difference solution of Laplace’s equation that is added so that their sum is a solution of Poisson’s equation in an infinite domain.²⁴ The procedure has the advantage that it is a direct method with a computational cost that is $O(n \log n)$ where n is the total number of grid points, and the bulk of the computational work is carried out by calls to efficient FFT routines.^{25,26} Other methods that are appropriate for uniform grids and utilize FFT routines for efficiency may also be considered.^{27–37} It is not difficult to imagine problems for which non-uniform grids are used to represent functions, or when the orbital basis functions have high frequency components. For such problems, the collection of methods such as adaptive Fast Multipole Methods (FMM)^{38,39} or adaptive fast convolution methods³² are possible choices. It is worth mentioning that for the test problem discussed in Sec. 4, the accuracy of the solution procedure used to solve Eq. (8) has been observed to have a significant impact on the precision with which the energies are determined.

2.2. Potential Dependent Orbital Basis

The construction of an approximate solution of the N -particle Schrödinger equation using Slater determinant basis functions requires a specification of a set of spatial orbitals. The use of a uniform grid and spectral approximations dictates that the basis functions be as smooth (differentiable) as possible. With the use of a computational grid, there is great flexibility in selecting basis functions, and in this section we describe a method for creating sets of orbitals that are adapted to the external potential and, assuming a smooth external potential, are also smooth.

The idea for the construction of these orbitals is an extension of the idea that underlies the use of hydrogenic orbitals as a basis for the classical description of atomic structure. Specifically, hydrogenic orbitals are the eigenfunctions of the single particle Schrödinger equation with the external potential being a single nuclear potential. These eigenfunctions are complete and, they, or smooth approximations to them, have proven to be exceptionally useful as basis sets for a variety of *ab initio* computational procedures. The extension of this idea in the context of semiconductor quantum dot modeling consists of using as an orbital basis the eigenfunctions of a single particle operator with the specified external potential. To induce complete localization of the orbital basis to the computational domain, two complementary additions, a barrier potential and a variable kinetic energy coefficient, are incorporated into the single particle operator. Specifically, the single particle operator used to construct the orbital basis has the form

$$h_b = -\frac{\hbar^2}{2} \nabla \cdot \beta_b(\mathbf{r}) \cdot \nabla + U_b(\mathbf{r}). \quad (9)$$

Here β_b is an augmented kinetic energy coefficient β , and U_b is U augmented by a domain boundary potential. The boundary potential is identically zero in the interior of the computational domain and smoothly transitions to having large positive value over the region of width b near the computational domain boundary. The additional boundary potential cannot be arbitrarily large for numerical reasons⁴⁰ so it cannot unconditionally localize all the eigenfunctions used for the orbital basis. To ensure localization, β_b is forced to transition from β to zero over the boundary region. Where the kinetic operator is zeroed, the Hamiltonian is completely local and disconnected from the interior of the domain. Hence all the low-energy eigenfunctions either do not encroach on or have vanishing tails outside of the computational domain.

The eigenfunctions are determined numerically as the orthonormal eigenvectors of a high order finite difference approximation to Eq. (9). The computation of the eigenvectors uses the same computational grid as that used for the orbital integrals. Since some of the eigenvalues and eigenvectors associated with this operator can be degenerate (and more so for the finite dimensional Hamiltonian of the FCI approximation itself), the use of a robust iterative method for determining the eigenpairs was necessary. The particular iterative method used to obtain the results presented here is the Rayleigh-Chebyshev method described in Ref. 41. We arbitrarily choose the M lowest eigenstates as the basis set, but

more elaborate strategies could be considered, possibly improving the convergence of FCI solutions.

3. BENCHMARK PROBLEM

In this section we describe the benchmark problem that demonstrates the construction of highly accurate solutions of the N -particle Schrödinger equations using a completely grid-based FCI procedure.

The problem chosen is an important one for the design of semiconductor qubits. Most implementations of semiconductor qubits use the electron spin as the fundamental quantum system that is manipulated; in some cases, the spin state itself is the qubit, in other cases, two low lying states of two or three electrons form the computational basis.³ For all of these cases, the electrons are confined in quantum dot nanostructures and, depending on how the qubit is defined, the controlled interaction between electron spins in neighboring dots is an important ingredient for either single or two qubit gates. This interaction usually takes the form of the Heisenberg exchange interaction, $H = J \mathbf{s}_1 \cdot \mathbf{s}_2$, where \mathbf{s}_1 and \mathbf{s}_2 are the spin states of electrons in neighboring dots. This interaction arises due to the overlap of the wave functions of the electrons in the two dots and can be controlled by changing the electron confining potential with voltages applied to surface gate electrodes. Faithful simulation of real devices requires detailed modeling of the semiconductor heterostructure potential, strain, and the electrostatic potential created by the gate electrodes through the solution — possibly self-consistent — of the Poisson equation with appropriate boundary conditions. Our method is fully compatible with using the results of an auxiliary calculation to provide the electron potential for use in the Schrödinger equation. However, such a calculation is not required to demonstrate the accuracy of our method, and so instead we use here an analytical potential representative of those formed in gated semiconductor devices.

An analytical expression⁴² for the potential generated beneath a row of several square gates of size $2a$ placed next to each other, each held at its own potential, with the surface outside the squares held at $V = 0$, is

$$\phi_0(x, y, z) = -\sum_i V_i \left[\begin{aligned} &g(a - x_i + x, a + y, z) + \\ &g(a - x_i + x, a - y, z) + \\ &g(a + x_i - x, a + y, z) + \\ &g(a + x_i - x, a - y, z) \end{aligned} \right] \quad (10)$$

where

$$g(u, v, z) = \frac{1}{2\pi} \tan^{-1} \left(\frac{uv}{z\sqrt{u^2 + v^2 + z^2}} \right). \quad (11)$$

Evaluating Eq. (10) for appropriate choices of the parameters creates the electron confining potential in two of the three directions, x and y , but along z another source of confinement is required. In real devices, it is commonly provided by a planar semiconductor heterostructure that utilizes two dissimilar materials, such as Si and a SiGe alloy, to form a one-dimensional (1D) quantum well for electrons. For the calculations described below, we assume the heteropotential of a

5 nm wide square well with a depth of 238 meV, typical numbers for a Si/SiGe heterostructure; it spans 15 nm in total to allow for some wave function penetration into a 5 nm barrier regions on either side of the well. The full 3D confining potential is then constructed here as a product of this 1D square well potential and the 2D potential, described by Eq. (10) at a specific depth \bar{z} corresponding to the middle of the quantum well. Other constructions are certainly possible, but found to be inconsequential for the present analysis.

We focus below on a case of two interacting electrons in a double quantum dot geometry. With only three gates total, we can shape the electrostatic confinement to form potential minima under the outer gates with a tunable barrier between them by varying gate voltages.

Figure 1 describes the model three-gate potential generated using Eq. (10) by setting $2a = \bar{z} = 70$ nm — typical for quantum dot qubit devices, $x_i = -2a, 0$, and $2a$, and the gate voltages $V_i = V_{P1}, V_X$, and V_{P2} to 0.25, 0.10, and 0.25 V, respectively. Panel (a) is a schematic of the three adjacent square gates. The dashed line cutting horizontally through the gates is at their midpoint and panel (b) shows a 1D slice of the potential taken along that cut. For these applied voltages, we see that two potential minima are formed under the outer gates with a small barrier under the middle gate, consistent with the outer gates being held at a slightly more positive bias than the middle gate. This is the configuration that quantum dot qubits typically operate in, where the barrier between the electrons is sufficient to keep them separated but still interacting through overlap of the tails of their wave functions. This interaction can be controlled in one of two ways — by modulating the height of the potential barrier through changing the voltage on the middle gate, V_X , or by changing the depth of one potential minimum relative to another, known as detuning, through asymmetrically biasing the outer gates, V_{P1} and V_{P2} . We will examine both of these modes of operation in the next section. Figure 1(c) shows the full 2D potential with the colors indicating its depth. The dashed line again corresponds to the location of the 1D cut shown in panel (b). The lateral dimensions of the computational domain are 300 nm for this case and for all the results below. While the potential has not fully relaxed to zero at the edge of the domain for these dimensions, note that its value at the edge is at least 25 meV above the bottom of the two potential minima. This is a rather deep confining potential for electrons in Si (with $m_x = m_y = 0.19m_0$, $m_z = 0.92m_0$, where m_0 is the free electron mass, and $\epsilon = 11.7\epsilon_0$ where ϵ_0 is the vacuum permittivity), and the ground state wave function of the single particle Schrödinger equation is effectively zero (below machine precision) well before reaching the edge of the domain. The modifications of the single particle Hamiltonian near domain boundaries, introduced in Eq. (9), ensure that all basis orbitals, including highly excited ones, vanish at the edge of the domain.

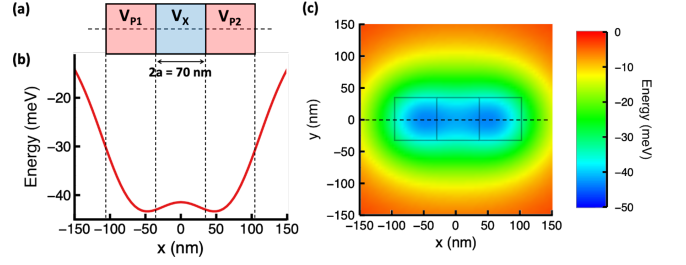


FIG. 1. (a) Schematic of the square gates used to generate the in-plane confining potential. (b) 1D slice of the model 2D confining potential taken at the midpoint of the gates as indicated by the dashed line in panel (a). (c) The full 2D potential with the color scale indicating its depth.

4. COMPUTATIONAL RESULTS

We first demonstrate the accuracy of our method by computing the exchange interaction in two-electron systems using the confining potential of the benchmark problem. The test consists of modulating the applied voltages so that the strength of the exchange interaction J varies from the peV to meV scales. For a two-electron system, the interpretation is straightforward in terms of total spin, and J is equal to the difference between energies of the lowest triplet and singlet states. Since the overall wave function must be antisymmetric as for any fermion system, the singlet (triplet) spatial part of the wavefunction is symmetric (antisymmetric) with respect to electron interchange, facilitating state attribution. This energy difference can get extremely small if the electrons are separated by a large potential barrier, meaning their spins become decoupled. With this background, we now can lay out the computational tasks (in fact, applicable to any number of electrons N) that must be performed for each bias:

- (i) Compute the lowest M eigenfunctions of the single particle operator in Eq. (9).
- (ii) Evaluate all one- and two-electron integrals associated with these M orbitals.
- (iii) For each distinct value of total spin projection S_z , construct the discrete N -electron Hamiltonian matrix from the corresponding subset of Slater determinants using the one- and two-electron integrals.
- (iv) Determine the eigenvalues and eigenvectors of the resulting Hamiltonian matrix.
- (v) *For two-electron exchange:* Take the difference between the lowest triplet and singlet to obtain J .

There are two types of errors associated with this computational procedure. The first type, the “numerical discretization error”, is the error associated with implementing discrete approximations for the differential and integral operators whose evaluation is required to set up and solve the equations. This

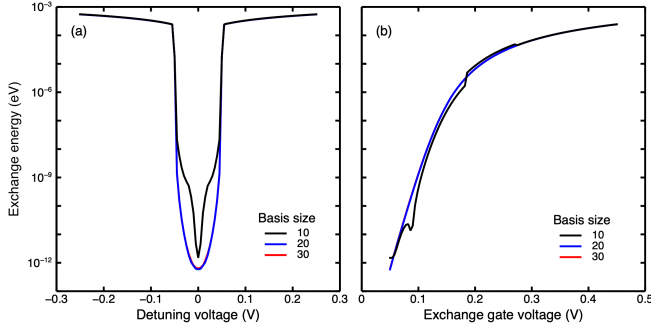


FIG. 2. Exchange energy calculated for different basis set sizes using the model potential described in the text. (a) J as a function of detuning voltage $V_{P2} - V_{P1}$ for exchange gate bias $V_X = 0.05$ V; at zero detuning, $V_{P1} = V_{P2} = 0.25$ V. (b) J versus V_X at zero detuning with $V_{P1} = V_{P2} = 0.25$ V.

includes also the error from approximating the orbitals numerically. The second type is the “orbital basis set error” due to approximating the desired N -particle eigenfunctions with a linear combination of Slater determinants formed from a *finite* set of spatial orbitals.

The potential associated with this benchmark problem is discontinuous in the z -direction at the quantum well interfaces, and, as a consequence, the order of accuracy of the integral and differential operators in the z -direction is reduced to second order (as long as the quantum well interfaces are coincident with computational grid planes). Since the order of accuracy in the in-plane directions is not affected, consistently accurate solutions can be obtained simply by using a more refined mesh in the out-of-plane direction. All the results presented below were obtained using a uniform mesh with 5 nm spacing in the x and y directions and 0.25 nm in the z direction.⁴³ The mesh spacings were chosen sufficiently small so that the dominant error in the exchange energy was due to orbital basis set size.

The orbital basis set is adaptive in the sense that every distinct bias (and hence device potential) can lead to a distinct set of orbital states that are used in the corresponding FCI calculation. Empirically we find that a relatively modest number of orbitals is sufficient for accurate calculation of the exchange energy.

Figure 2(a) shows the calculated exchange energy as a function of detuning voltage at a fixed exchange gate bias $V_X = 0.05$ V. The detuning voltage is defined as the difference between V_{P2} and V_{P1} . Although this is just a model potential, these detunings are in the range of what is applied to real devices to achieve practical values of exchange energy. The data shown is for three different basis set sizes, 10, 20, and 30. The basis functions themselves are the eigenstates of the single particle Hamiltonian as described in Eq. (9). For large values of detuning, J is on the order of a few hundred μ eV and varies weakly with bias, representing the situation when the two electrons collapse into the same dot. The suppression of J at smaller values of detuning is due to the two electrons becoming spatially separated into the left and right dots with a potential barrier between them. The abruptness

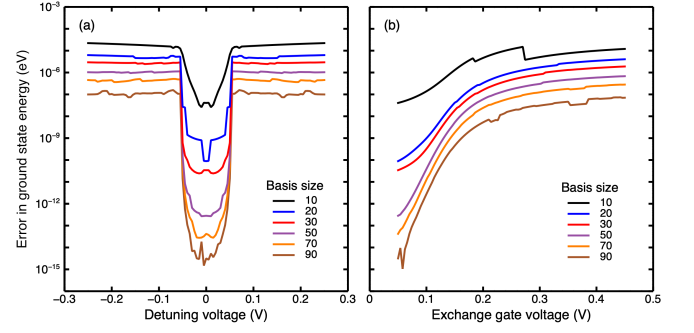


FIG. 3. Absolute error in the ground state energy E_0 as the (a) detuning and (b) exchange gate voltages are varied. For each reported basis set size, it is estimated as a difference in E_0 with value calculated using basis set size of 100.

of this transition depends on the exchange gate voltage, V_X . For larger V_X , the interdot barrier is reduced, the minimum exchange increases and this transition is more gradual. We chose the case in Fig. 2(a) because it highlights that we are able to achieve well-converged energies even at the peV scale. Indeed, with only 20 basis functions, the exchange energy is already well-converged and increasing the basis set size does not significantly change the results on an absolute scale. Good convergence over more than 8 orders of magnitude in J is due to using an adaptive basis which is the hallmark of our approach. While convergence over such a large range may not be necessary in other cases, it is actually quite important for modeling semiconductor qubits. Controlling the exchange interaction over this range is essential to the operation of these devices. For example, knowing that the minimum value of J (the so-called residual exchange) for a particular set of voltages is, say, 10 peV rather than 1 neV can be the difference between a functional and a faulty qubit tune-up (or even design), as large residual exchange causes significant errors in qubit operation that are not easily corrected.

Figure 2(b) shows J as a function of exchange gate bias V_X at zero detuning with $V_{P1} = V_{P2} = 0.25$ V; this modulation keeps the potential symmetric along x and the dots singly occupied, resulting in a smoother variation of J compared to the detuning case. The exchange energy is approximately exponential in V_X at lower voltages where the potential barrier is large and only the tails of the electron wave functions are interacting. The simplest theories for barrier tunneling explain this behavior⁴⁴ and are confirmed here in a more complex potential. At larger V_X values, the potential barrier is nearly zero; in this regime, the two electrons end effectively in one large, shallow potential well and a saturation of J is expected. As was already observed for the detuning case, the calculation converges quickly with basis set size and is well converged across the whole range of J values.

What we have demonstrated so far is convergence with respect to basis set size on an absolute scale, meaning that we can compute the exchange energy over a very large range and be confident that the calculation is not off by a significant factor even for extremely small values of J provided that the basis set is sufficiently large, e.g., greater than 20. The plots shown

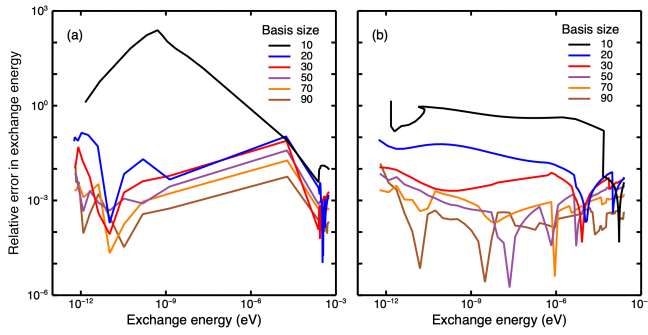


FIG. 4. Relative error in exchange energy J for (a) detuning and (b) exchange gate voltage sweeps. Shown for several basis set sizes as a function of J calculated using a basis set size of 100.

give very little indication of the relative error in J , however.

The exchange energy is determined by the difference of the two lowest energy values, and we turn next to estimating the accuracy with which the energies themselves are being computed. Exact values for the energies of the system are not known, and so an estimate of the error is obtained by comparing the results of computations with orbital basis sets of sizes from 10 to 90 with those obtained with the largest basis set of size 100. Figure 3(a) and (b) show the values of the estimated error for the overall ground state (which is a singlet) energy as the detuning and exchange biases are varied. For every bias, the energy values converge monotonically as the basis set sizes increases. The behavior of the estimated error of the first excited state (which is the ground triplet) was similar and so is not shown. A prominent feature in these results is that the convergence behavior is not uniform with respect to bias voltages. In particular, as the biases are varied so J decreases, the estimated accuracy of the energies improves. This behavior can be explained by the observation that as J decreases, the configuration tends to one whose electronic structure is associated with two spatially separated electrons interacting primarily electrostatically. Since the orbital basis used consists of eigenfunctions of the single particle operator, one expects more rapid convergence. The second feature, abrupt jumps in the estimated errors, is because we elected to use the M lowest eigenstates as the basis set. This can lead to inclusion or exclusion of an important orbital when its energy dips or rises relative to other states, and is most extreme at smallest M .

Figure 4(a) and (b) shows the estimated relative error in J for the detuning and exchange gate voltage sweeps for basis sets of size between 10 and 90. The error is defined as the absolute value of the difference between J extracted for a given basis set size and a basis size of 100, divided by the value of J for basis size of 100 (which is also used as the abscissa value). This data shows that, aside from the basis size of 10, which is obviously not well converged as shown in the previous plots, the relative error is generally within a few percent, and, using larger basis sets, can readily be pushed below one percent over the entire range of J . Since J is computed by subtracting two nearly equal energy values, the constraints of finite precision arithmetic and computed eigenvalue accuracy set a floor on the resolvable relative error in J . Thus, for the smallest values

of J the non-monotonic trend of the relative errors as the basis size increases is not unexpected.

5. CONCLUSION

This paper describes a collection of discretization techniques that can be combined to create a real space, grid based method for the determination of energies and wave functions of the N -particle Schrödinger equation used to approximate electrostatically confined electron states in semiconductor quantum dots. In this method, both high order finite difference and spectral approximations of differential and integral operators are used to obtain high accuracy. High computational efficiency for the evaluation of the two-electron integrals is obtained through the use of high performance fast Fourier transform routines.^{25,26} The use of completely grid-based approximations facilitates use of numerically determined orbital basis functions. In particular, one can construct and utilize orthonormal orbital basis sets that consist of eigenfunctions of a single particle operator with arbitrarily defined external potentials. This capability allows for the creation of adaptive orbital basis sets for problems in which the external potential varies greatly.

A benchmark problem is presented that incorporates an analytically described confining potential representative of potentials produced in electrostatically gated devices. The computational results demonstrate that when our method is applied to the benchmark problem, the energy differences between the ground singlet and triplet two-electron states are accurate to within a percent over a wide range of model parameters and resulting exchange values.

While the use of the discretization techniques has been demonstrated for the implementation of a FCI procedure for electrons in a semiconductor, the same techniques can certainly be utilized in other problems, for example standard molecular modeling,⁴⁵ or implementations of other *ab initio* procedures such as Hartree-Fock or density functional theory.⁴⁶ They may also find application in the construction of methods that necessitate the use of real-space grids, in particular, methods that combine different types of quantum mechanical approximations in different regions of physical space.

ACKNOWLEDGMENTS

We would like to acknowledge Ekmel Ercan for careful reading of the manuscript. This work was supported in part by the DARPA Quantum Information Science and Technology (QuIST) Program (ARO DAAD-19-01-C-0077).

AUTHOR DECLARATIONS

Conflict of interest

The authors have no conflicts to disclose.

DATA AVAILABILITY

Data available on request from the authors.

REFERENCES

- ¹R. Hanson, L. P. Kouwenhoven, J. R. Petta, S. Tarucha, and L. M. K. Vandersypen, *Rev. Mod. Phys.* **79**, 1217 (2007).
- ²F. A. Zwaneburg, A. S. Dzurak, A. Morello, M. Y. Simmons, L. C. L. Hollenberg, G. Klimeck, S. Rogge, S. N. Coppersmith, and M. A. Eriksson, *Rev. Mod. Phys.* **85**, 961 (2013).
- ³G. Burkard, T. D. Ladd, J. M. Nichol, A. Pan, and J. R. Petta, (2021), arXiv:2112.08863 [cond-mat.mes-hall].
- ⁴M. D. Reed, B. M. Maune, R. W. Andrews, M. G. Borselli, K. Eng, M. P. Jura, A. A. Kiselev, T. D. Ladd, S. T. Merkel, I. Milosavljevic, E. J. Pritchett, M. T. Rakher, R. S. Ross, A. E. Schmitz, A. Smith, J. A. Wright, M. F. Gyure, and A. T. Hunter, *Phys. Rev. Lett.* **116**, 110402 (2016).
- ⁵M. Friesen, P. Rugheimer, D. E. Savage, M. G. Lagally, D. W. van der Weide, R. Joynt, and M. A. Eriksson, *Phys. Rev. B* **67**, 121301 (2003).
- ⁶M. Rontani, C. Cavazzoni, D. Bellucci, and G. Goldoni, *J. Chem. Phys.* **124**, 124102 (2006).
- ⁷A. Tankasala, J. Salfi, J. Bocquel, B. Voisin, M. Usman, G. Klimeck, M. Y. Simmons, L. C. L. Hollenberg, S. Rogge, and R. Rahman, *Phys. Rev. B* **97**, 195301 (2018).
- ⁸B. Joecker, A. D. Baczewski, J. K. Gamble, J. J. Pla, A. Saraiva, and A. Morello, *New Journal of Physics* **23**, 073007 (2021).
- ⁹S. M. Reimann and M. Manninen, *Rev. Mod. Phys.* **74**, 1283 (2002).
- ¹⁰H. E. Ercan, S. N. Coppersmith, and M. Friesen, *Phys. Rev. B* **104**, 235302 (2021).
- ¹¹J. C. Abadillo-Uriel, B. Martinez, M. Filippone, and Y.-M. Niquet, *Phys. Rev. B* **104**, 195305 (2021).
- ¹²E. Nielsen, R. W. Young, R. P. Muller, and M. S. Carroll, *Phys. Rev. B* **82**, 075319 (2010).
- ¹³M. A. Bakker, S. Mehl, T. Hiltunen, A. Harju, and D. P. DiVincenzo, *Phys. Rev. B* **91**, 155425 (2015).
- ¹⁴R. Rahman, E. Nielsen, R. P. Muller, and M. S. Carroll, *Phys. Rev. B* **85**, 125423 (2012).
- ¹⁵J. I. Climente, A. Bertoni, M. Rontani, G. Goldoni, and E. Molinari, *Phys. Rev. B* **74**, 125303 (2006).
- ¹⁶K. Deng and E. Barnes, *Phys. Rev. B* **102**, 035427 (2020).
- ¹⁷A. Pan, T. E. Keating, M. F. Gyure, E. J. Pritchett, S. Quinn, R. S. Ross, T. D. Ladd, and J. Kerckhoff, *Quantum Science and Technology* **5**, 034005 (2020).
- ¹⁸E. Nielsen, R. Rahman, and R. P. Muller, *Journal of Applied Physics* **112**, 114304 (2012), <https://doi.org/10.1063/1.4759256>.
- ¹⁹A. Secchi, L. Bellentani, A. Bertoni, and F. Troiani, *Phys. Rev. B* **104**, 035302 (2021).
- ²⁰With spatially varying effective mass, order of operators in the kinetic term of Eq. (1) is important. As written, it does preserve Hamiltonian hermiticity, but the formulation is actually not unique. For a broader view on the physical origins of the material dependent effective mass, complying Hamiltonian formulations, compatible boundary conditions at heterointerfaces, and their repercussions for electron states in heterostructures see Ref. 47. Using a single macroscopic dielectric constant is an approximation which can break down at the atomic scale (due to dielectric screening effects) or near heterointerfaces where disparate materials with different dielectric constants meet, in which cases the Coulomb interaction can be adjusted to incorporate additional physics^{48,49}.
- ²¹A. Szabo and N. S. Ostlund, *Modern quantum chemistry*, Dover Books on Chemistry (Dover Publications, Mineola, N.Y., 1996).
- ²²K. Atkinson, *An introduction to numerical analysis*, 2nd ed. (Wiley, New York, 1988).
- ²³The values outside the computational domain that are required for the evaluation of the finite difference operator at points near the boundaries are taken to be identically zero; these values are consistent with the assumption that the spatial orbitals vanish outside the computational domain.
- ²⁴C. R. Anderson, (2021), arXiv:2108.11871 [math.NA].
- ²⁵M. Frigo and S. Johnson, *Proceedings of the IEEE* **93**, 216 (2005).
- ²⁶M. Frigo and S. G. Johnson, <http://www.fftw.org/> (2014), FFTW 3.3.4.
- ²⁷R. James, *Journal of Computational Physics* **25**, 71 (1977).
- ²⁸P. McCorquodale, P. Colella, G. Balls, and S. Baden, in *2005 International Conference on Parallel Processing Workshops (ICPPW'05)* (IEEE).
- ²⁹P. McCorquodale, P. Colella, G. Balls, and S. Baden, *Communications in Applied Mathematics and Computational Science* **2**, 57 (2007).
- ³⁰D. B. Serafini, P. McCorquodale, and P. Colella, *Journal of Physics: Conference Series* **16**, 481 (2005).
- ³¹Z. Wang, *Journal of Computational Physics* **153**, 666 (1999).
- ³²G. Beylkin, C. Kurcz, and L. Monzón, *Journal of Computational Physics* **228**, 2770 (2009).
- ³³F. Vico, L. Greengard, and M. Ferrando, *Journal of Computational Physics* **323**, 191 (2016).
- ³⁴L. Exl, N. J. Mauser, and Y. Zhang, *Journal of Computational Physics* **327**, 629 (2016).
- ³⁵C. A. Rozzi, D. Varsano, A. Marini, E. K. U. Gross, and A. Rubio, *Phys. Rev. B* **73**, 205119 (2006).
- ³⁶M. M. Hejlesen, J. T. Rasmussen, P. Chatelain, and J. H. Walthers, *Journal of Computational Physics* **252**, 458 (2013).
- ³⁷M. M. Hejlesen and J. H. Walthers, *Journal of Computational Physics* **326**, 188 (2016).
- ³⁸H. Langston, L. Greengard, and D. Zorin, *Communications in Applied Mathematics and Computational Science* **6**, 79 (2011).
- ³⁹D. Malhotra and G. Biros, *Communications in Computational Physics* **18**, 808 (2015).
- ⁴⁰Using a very large positive value for the potential increases the spectral radius of the operator whose eigenvectors are used to create the basis. If Krylov subspace iterative methods, such as the Rayleigh-Chebyshev method used in this paper,⁴¹ are employed, then an increase in spectral radius can substantially reduce the computational efficiency of the iterative procedure for determining the eigenvectors.
- ⁴¹C. R. Anderson, *Journal of Computational Physics* **229**, 7477 (2010).
- ⁴²J. H. Davies, I. A. Larkin, and E. V. Sukhorukov, *Journal of Applied Physics* **77**, 4504 (1995).
- ⁴³Using the domain dimensions stated above, 300 nm in the in-plane directions and 15 nm along z , this results in a total of $n = 226981$ points that define the computational grid. This is therefore the size of the system that defines the discretized single particle Hamiltonian and associated orbital basis states which are integrated over to obtain the orbital matrix elements.
- ⁴⁴S. K. Bhattacharya and A. R. P. Rau, *Physical Review A* **26**, 2315 (1982).
- ⁴⁵C. R. Anderson, *The Journal of Chemical Physics* **148**, 114111 (2018).
- ⁴⁶R. M. Martin, *Electronic Structure* (Cambridge University Press, 2004).
- ⁴⁷E. L. Ivchenko and G. E. Pikus, *Superlattices and Other Heterostructures: Symmetry and Optical Phenomena*, 2nd ed. (Springer-Verlag, Berlin, 1997).
- ⁴⁸D. R. Penn, *Phys. Rev.* **128**, 2093 (1962).
- ⁴⁹M. V. Fischetti and S. E. Laux, *Journal of Applied Physics* **89**, 1205 (2001).